30. T. G. Martin, S. McIntyre, C. P. Catterall, H. P. Possingham, *Biol. Conserv.* **127**, 201–214 (2006).
31. O. Hoegh-Guldberg *et al.*, *Science* **321**, 345–346 (2008).
32. H. Yokomizo, H. P. Possingham, P. E. Hulme, A. C. Grice, Y. M. Buckley, *Biol. Invasions* **14**, 839–849 (2012).

ACKNOWLEDGMENTS

We thank the personnel of the Invasive *Spartina* Project, including P. Olofson, E. Grijalva, D. Kerr, I. Hogle, W. Thornton, M. Latta, and others, who provided data on *Spartina* distributions, clapper rail populations, and costs of eradication and restoration efforts. We thank D. Kling for research assistance and P. Reynolds for comments on the manuscript. We thank the California State Coastal Conservancy and the California State Wildlife Conservation Board for use of their data. The data used for this paper are summarized in table S1 (*24*) and are given in more detail in (*24*). This research was supported by NSF grant no. DEB 1009957 to A.H., E.D.G., J.N.S., A.L., and S.L.J.

SUPPLEMENTARY MATERIALS

www.sciencemag.org/content/344/6187/1028/suppl/DC1
Materials and Methods
Supplementary Text
Figs. S1 to S6
Tables S1 to S4
References (*33*–*46*)

13 January 2014; accepted 23 April 2014
10.1126/science.1250763

CELLULAR DYNAMICS

High-resolution mapping of intracellular fluctuations using carbon nanotubes

Nikta Fakhri,[1] Alok D. Wessel,[1] Charlotte Willms,[1] Matteo Pasquali,[2] Dieter R. Klopfenstein,[1] Frederick C. MacKintosh,[3]* Christoph F. Schmidt[1]*

Cells are active systems with molecular force generation that drives complex dynamics at the supramolecular scale. We present a quantitative study of molecular motions in cells over times from milliseconds to hours. Noninvasive tracking was accomplished by imaging highly stable near-infrared luminescence of single-walled carbon nanotubes targeted to kinesin-1 motor proteins in COS-7 cells. We observed a regime of active random "stirring" that constitutes an intermediate mode of transport, different from both thermal diffusion and directed motor activity. High-frequency motion was found to be thermally driven. At times greater than 100 milliseconds, nonequilibrium dynamics dominated. In addition to directed transport along microtubules, we observed strong random dynamics driven by myosins that result in enhanced nonspecific transport. We present a quantitative model connecting molecular mechanisms to mesoscopic fluctuations.

The cytoplasm of eukaryotic cells is a highly dynamic composite polymer material. Its mechanical properties are dominated by protein polymers: microtubules (MTs), F-actin, and intermediate filaments (*1*–*4*). Metabolism maintains a chemical nonequilibrium that energizes this mechanical framework of cells. Dominant driving forces stem from the polymerization of actin and tubulin and from motor proteins, both deriving energy from nucleotide triphosphate hydrolysis (*5*, *6*). Molecules self-organize into complex machineries on all scales to drive functions as various as intracellular transport, cell locomotion, and muscle contraction. Understanding these machineries requires observing intracellular dynamics from molecular to macroscopic scales. Fluorescence microscopy allows labeling of specific targets, but it has been impossible to achieve long-term tracking of single molecules because of the fluorescent background in cells and fluorophore instabilities. Observations of intramolecular dynamics have often used mesoscopic endogenous particles or ingested beads (*7*, *8*) instead of molecular tracers.

Generally, dynamics in cells are scale-dependent. At short times (microseconds to milliseconds), thermal motions should dominate. Between milliseconds and seconds, thermal diffusion might still be relevant, but there is mounting evidence, both in vitro and in vivo, that the motion of larger objects couples to myosin-driven stress fluctuations in the cytoskeleton (*9*, *10*). Here, temporal fluctuations, reminiscent of thermal diffusion in liquids, can arise from nonequilibrium dynamics in the viscoelastic cytoskeleton (*11*). On longer time scales, from minutes to hours, directed transport and larger-scale collective motions typically dominate. The motion of probe particles tracked inside cells has been classified as subdiffusive, diffusive, or superdiffusive. Such classifications, however, obscure the distinction between thermally driven and nonequilibrium fluctuations and are inadequate to identify intracellular material properties.

Motor proteins are good reporters of dynamics from the molecular scale upward because they drive many cellular motions. Kinesins and myosins have been extensively studied in vitro (*12*, *13*), but the dynamics of motors in cells remain largely unexplored (*14*). Following motor motion in cells by fluorescence microscopy requires (i) stable, nonbleaching fluorescent probes, (ii) high signal-to-noise ratio in imaging, and (iii) efficient targeting of probes to specific molecules. Modern optical equipment in conjunction with optimized fluorescent dyes can resolve and track single molecules with high temporal and spatial resolution in vitro (*15*). In living cells, however, molecular imaging has been limited to short times (~1 s)—for example, in superresolution microscopy (*16*). Moreover, signal-to-noise ratios tend to be marginal because of cellular background fluorescence.

Here, we used single-walled carbon nanotubes (SWNTs) as a tool for high-bandwidth intracellular tracking. SWNTs are stiff quasi–one-dimensional tubular all-carbon nanostructures with diameters of ~1 nm and persistence lengths above 10 μm (*17*). Individual semiconducting SWNTs luminesce with large Stokes shifts in the near-infrared (900 to 1400 nm) (*18*). This window is virtually free of autofluorescence in biological tissues. Fluorescence emission is highly stable with no blinking and negligible photobleaching (*19*, *20*) (fig. S1), allowing for long-term tracking (*21*). The fluorescence lifetime is short [~100 ps (*22*)] so that high excitation intensities allow millisecond time resolution.

To track the dynamics of the cytoskeleton without introducing invasive probes, we specifically targeted short SWNTs (~100 to 300 nm; fig. S2) to the endogenous kinesin-1 motor Kif5c in cultured COS-7 cells (see supplementary materials). Kif5c functions as a cargo transporter in cells (*23*). We dispersed SWNTs by wrapping with short DNA oligonucleotides and used HaloTag (*24*) to covalently attach SWNTs specifically to full-length kinesins expressed in the cells (Fig. 1, A and B). We used an additional green fluorescent protein label to confirm localization and motility of the motors on MTs (figs. S3 and S4 and movie S1). Tracking motor proteins makes it possible to observe several types of dynamics. Besides observing directed kinesin-driven transport on MTs, it is possible to directly observe fluctuations of the MT network because a moving kinesin must be bound to a MT. The MT tracks are embedded in the viscoelastic actin cytoskeleton, which in turn fluctuates as a result of stresses generated by cytoplasmic myosins (Fig. 1C) (*25*, *26*).

The high photostability of SWNTs made it possible to introduce only a small number, around 100 per cell, and still track individual SWNTs

[1]Drittes Physikalisches Institut–Biophysik, Georg-August-Universität, 37077 Göttingen, Germany. [2]Department of Chemical and Biomolecular Engineering, Department of Chemistry, Smalley Institute for Nanoscale Science and Technology, Rice University, Houston, TX 77005, USA. [3]Department of Physics and Astronomy, Vrije Universiteit, 1081 HV Amsterdam, Netherlands.
*Corresponding author. E-mail: christoph.schmidt@phys.uni-goettingen.de (C.F.S.); fcmack@gmail.com (F.C.M.)

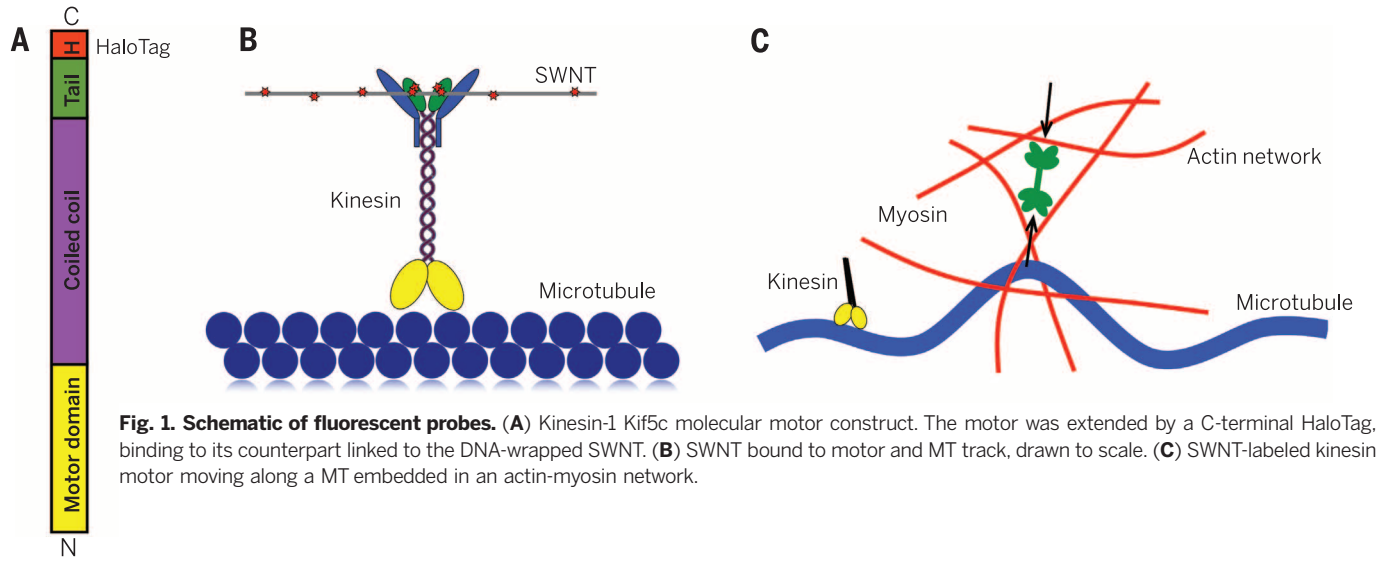

Fig. 1. Schematic of fluorescent probes. (**A**) Kinesin-1 Kif5c molecular motor construct. The motor was extended by a C-terminal HaloTag, binding to its counterpart linked to the DNA-wrapped SWNT. (**B**) SWNT bound to motor and MT track, drawn to scale. (**C**) SWNT-labeled kinesin motor moving along a MT embedded in an actin-myosin network.

Fig. 2. Tracking SWNT-labeled kinesins in COS-7 cells. (**A**) Tracks of SWNT-labeled kinesin-1 motors (Kif5c) in a COS-7 cell shown as 2D maximum-intensity projection (movie S2). Nucleus and cell periphery are outlined with red dashed and dotted lines, respectively. Red diamonds mark beginning and end of the 8.3-min trajectory of a particular SWNT-kinesin. (**B**) Kymograph of a single SWNT-labeled kinesin tracked over ~40 μm [track marked by red diamonds in (A)]. (**C**) Track of a SWNT-labeled kinesin in a cell; frame time, 5 ms (movie S4). (**D**) Histogram of the magnitude of velocity of SWNT-labeled kinesins, averaged over 2-s segments (N = 367 in 30 cells). The inset is a single frame of individual SWNT-labeled kinesins showing high image contrast. Heat map color code indicates relative intensity.

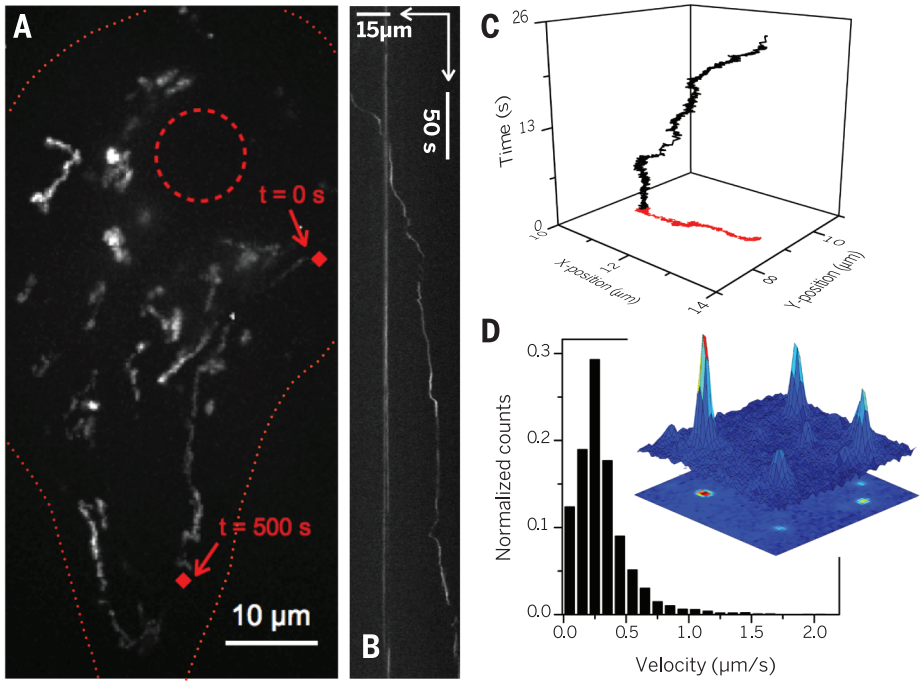

for up to 1.5 hours. We used a single-molecule tracking algorithm (*27*) and determined the centroid position of SWNTs in the focal plane to a precision of 20 to 50 nm. Fluorescent spots were detected with a signal-to-noise ratio of about 20 (for integration times of 60 to 250 ms; Fig. 2D, inset, and fig. S5). In typical recordings, we observed up to 30% of SWNTs moving in a directed manner, with the rest moving randomly but remaining locally constrained. Occasionally, random motion turned into directed motion and vice versa. These cases confirm that the label was attached to a motor, which in turn was attached to a MT. Tracks of the moving SWNTs (Fig. 2A) showed long and relatively straight unidirectional runs, typical for kinesin-1. The average velocity of straight runs, low-pass filtered over segments of 2 s, was 300 ± 210 nm/s (mean ± SD), consistent with previous reports (*28*, *29*) (Fig. 2D), confirming largely unimpeded motility. Several SWNT-labeled kinesins could be tracked across the whole cell, much farther than the average run length (~1 μm) of a single kinesin-1 in vitro (*30*) (Fig. 2A and fig. S6). This suggests that the labeled motors were attached to cargo vesicles with other motors. Motors generally moved in a stop-and-go fashion (Fig. 2B). Pauses might reflect temporary detachment or mechanical obstacles (*31*). During phases of movement, kinesin velocity varied in magnitude and direction, predominantly pointing toward the cell periphery (Fig. 2A).

The photostability of SWNTs also made it possible to increase the time resolution by increasing illumination intensity without sacrificing overall recording time. To capture short-time dynamics, we imaged with a time resolution of 5 ms per frame (Fig. 2C and movie S4). With this resolution, we analyzed the randomly moving population (Fig. 3A, inset) by computing the mean squared displacement (MSD) of trajectories, $\langle \Delta r^2(\tau) \rangle$, where τ is the lag time and $\Delta r(\tau) = r(t + \tau) - r(t)$ is the distance traveled in the focal plane in time τ. The MSD grows with lag time, typically exhibiting approximate power-law behavior $\langle \Delta r^2(\tau) \rangle \propto \tau^{\alpha}$. The MSD exponent α, which may vary from one to another time regime, provides an important characteristic of the motion. For observation times between 5 ms and 2.5 s, we found an averaged MSD transitioning from $\alpha \approx 0.25$ to $\alpha \approx 1$ (Fig. 3B).

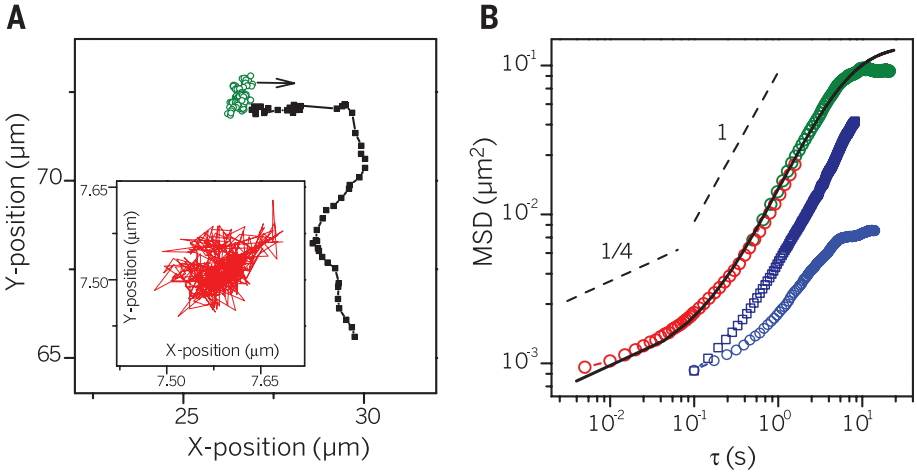

Fig. 3. Nonequilibrium stirring of the cytoplasm. (**A**) 2D projection of a SWNT-labeled kinesin trajectory initially moving randomly (stationary phase, green circles) and then moving on MTs; frame time, 250 ms (black squares). The inset shows the trajectory of a SWNT-labeled kinesin with frame time of 5 ms. (**B**) Average 2D MSD of the motor during the stationary phase at frame times of 250 ms (green circles, $N = 10$) and 5 ms (red circles, $N = 10$). A noise floor is subtracted (fig. S12 and supplementary materials). Approximate power-law slopes of 0.25 and 1 are indicated. Same after treatment with blebbistatin (dark blue squares, 10 μM blebbistatin, $N = 5$; blue circles, 50 μM blebbistatin, $N = 5$). The black line is the model curve, the weighted sum of Eqs. 3 and 4. The following values for the parameters (in addition to weights) have been chosen to best approximate the data: $\beta = 0.2$, $\tau_c = 5$ s.

Next we analyzed longer trajectories recorded with a 250-ms frame time. When random motion turned into directed motion (Fig. 3A), we could be sure that we were observing SWNTs attached to motors. We separately analyzed the stationary and directed segments of those trajectories. The MSDs from stationary segments showed a scaling exponent $\alpha = 1.1 \pm 0.2$ (Fig. 3B) for intermediate times, connecting in slope and amplitude to the short-time MSDs, and then leveling off for $\tau > 5$ to 10 s. Motors might have been unbound from MTs during the stationary segments. To exclude ambiguity, we also analyzed the directed-motion segments of the tracks. The fact that MTs are locally straight allowed us to distinguish track fluctuations by decomposing trajectories into longitudinal (on-axis) and transverse (off-axis) components (Fig. 4A). Longitudinal motion showed a MSD with $\alpha \approx 2$ at long times, confirming processive motor motion (Fig. 4, B and D), while the transverse MSD again showed an exponent $\alpha \approx 1$ for intermediate times. The transverse MSD also leveled off for times longer than 5 to 10 s, just as the MSD from the stationary segments (Fig. 4, B to D). To test whether there was a mutual dependency between the speed of directed transport and the off-axis fluctuations, we correlated on-axis velocity and off-axis displacement variance in time windows of 0.5 s (fig. S7). There was no apparent correlation, except for a slight decrease in variance at the highest velocities measured (>750 nm/s), which is likely to be an artifact. As a control, we also introduced functionalized SWNTs into COS-7 cells that did not express HaloTag kinesins (fig. S8 and movie S3). In those cells, we did not observe MSDs with $\alpha \approx 2$, but for roughly half of the tracked SWNTs, we did observe the active exponent of $\alpha \approx 1.2$ while the remainder of SWNTs were less mobile (fig. S9).

Thus, the active transverse MT fluctuations are not due to kinesin motors, but instead reflect the dynamics of the cytoskeleton. The way the relatively rigid MTs report these dynamics depends on two restoring forces: the elastic force of bent MTs and the force exerted by the strained cytoskeletal matrix in which the MTs are embedded. Because it is hard to bend an elastic rod on short length scales, the surrounding matrix yields to the MT when it is deformed on short length scales. By contrast, the MT yields to matrix forces for deflections of wavelength larger than ~1 μm (*32*). The shorter-wavelength MT deflections relax faster than our 5-ms frame rate (*5*). Therefore, we assume that the transverse MT motion we observe reflects the (active or passive) strain fluctuations of the surrounding matrix.

The MSD power-law exponent α generally reflects the randomness of motion. More precisely, in any medium, the MSD of an embedded probe particle is governed both by the material properties of the medium and the temporal characteristics of the forces driving the particle. For thermally driven Brownian motion in simple liquids, the MSD exponent $\alpha = 1$. For thermal motion in viscoelastic media, which exhibit time- and frequency-dependent viscosity and elasticity, $\alpha < 1$ strictly holds. For viscoelastic materials, the stiffness $G(\omega)$ typically increases with a power of frequency ω: $G(\omega) \propto \omega^{\beta}$. This is observed in polymer solutions, where the viscoelastic exponent $\beta \approx 0.5$ to 0.8 (*33*), as well as in cells, where $\beta \approx 0.1$ to 0.2 on time scales on the order of seconds (*34*). This value of the exponent is close to what is expected for purely elastic materials, where $\beta = 0$. The nearly elastic behavior of cells can be understood as a consequence of strong cross-linking in the cytoskeleton. Knowing the driving forces, it is possible to construct a relation between MSD exponent α and viscoelastic exponent β. For thermal driving forces, the MSD exponent $\alpha = \beta$ (*9*). Thermal fluctuations can therefore never appear as "superdiffusive" motion with $\alpha > 1$. Nonthermal driving, by contrast, can result in superdiffusive motion. Theory provides a specific prediction for motion in nearly elastic solids driven by random stress fluctuations with long correlation times and sudden transitions: $\alpha = 1 + 2\beta$ (*11*, *35*, *36*). This prediction is expected to apply for cytoskeletal stress fluctuations caused by randomly distributed cytoplasmic myosin minifilaments. Myosin locally contracts the actin network with an attachment time of several seconds, followed by sudden release. Some hints of this predicted scaling have been reported for cells and reconstituted acto-myosin model systems (*9*–*11*, *35*). When $\beta = 0$ (i.e., in the elastic limit), the resulting MSDs can look deceptively like Brownian motion in a simple liquid, although the physical reason is entirely different. For observation times τ longer than the correlation time of the driving forces, the MSD is predicted to level off (*11*), as we observed. In our experiments, the stress correlation time should correspond to typical cytoplasmic myosin motor engagement times, which are indeed reported to be ~10 s in cells.

We modeled the entire expected MSD curves to match asymptotic power-law segments and to also capture the transitions between the different regimes we observed. For a medium with shear stiffness $G(\omega)$, the frequency-dependent displacement $r(\omega)$ is proportional to applied force $f(\omega)$ and inversely proportional to $G(\omega)$. Thus, the power spectral density (PSD) of r is given by

$$\langle r^2\rangle_\omega = \int \langle r(t+\tau)r(t)\rangle \exp(i\omega\tau)d\tau \propto \frac{\langle f^2\rangle_\omega}{|G(\omega)|^2} \quad (1)$$

For active forces governed by a correlation time τ_c, the force spectrum is predicted to be

$$\langle f^2\rangle_\omega = \int \langle f(t)f(0)\rangle \exp(i\omega\tau)dt \propto \frac{1}{1+(\omega\tau_c)^2} \quad (2)$$

(*11*, *35*). This spectrum corresponds, in the time domain, to a net force due to randomly distributed myosins that grows as a random walk in time $\langle \Delta f^2(\tau)\rangle \propto \tau$ for times less than τ_c, and looks like white, uncorrelated noise at longer times (*37*). Thus, the active MSD is

$$\langle \Delta r^2(\tau)\rangle_{\text{active}} \propto \int [1 - \exp(-i\omega\tau)] \frac{1}{[1+(\omega\tau_c)^2]|G(\omega)|^2} \frac{d\omega}{2\pi} \quad (3)$$

(see supplementary materials). By contrast, the passive MSD is given by

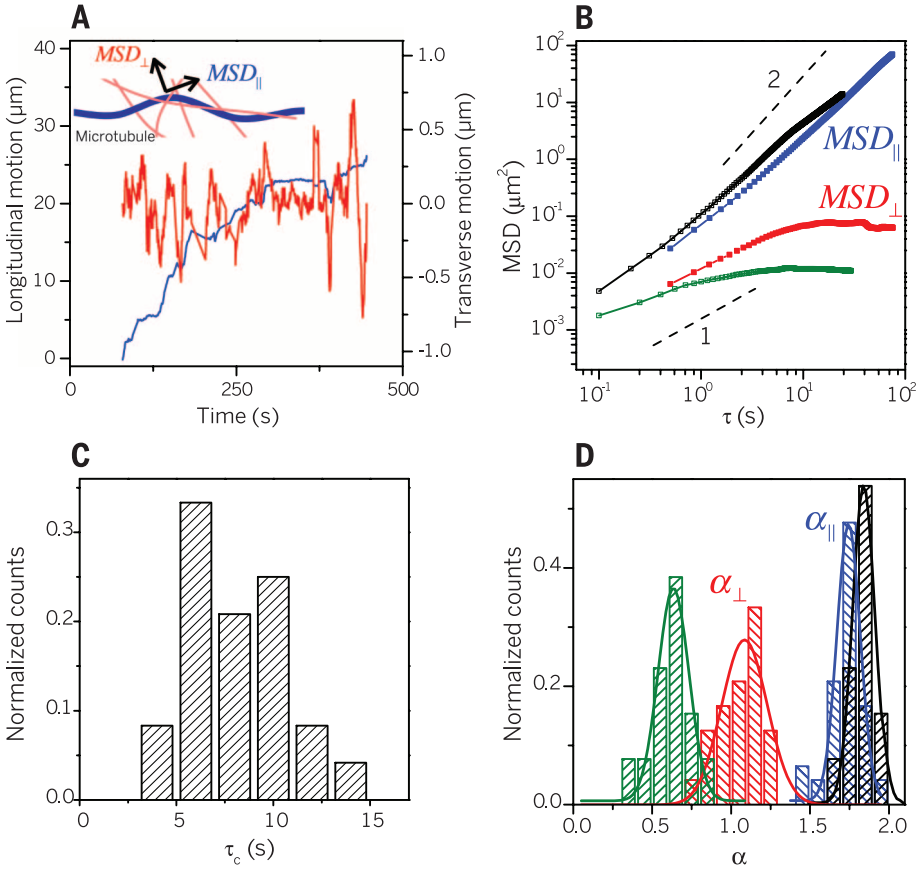

Fig. 4. Kinesin tracking on MTs buffeted by myosin. (**A**) Decomposition of a motor trajectory into longitudinal (blue) and transverse (red) components relative to the MT tangent. (**B**) Average MSD of longitudinal (blue squares, N = 5) and transverse (red squares, N = 5) components of a run. Same after treatment with 50 μM blebbistatin, transverse (green open squares, N = 7) and longitudinal (black open squares, N = 7). Power-law slopes are indicated. (**C**) Histogram of characteristic leveling-off times τ_c of the transverse MSDs, representing myosin correlation time (N = 30). (**D**) Histogram of MSD scaling exponents at intermediate times for longitudinal (blue) and transverse (red) components for motors moving processively along MTs (N = 30). After treatment with 50 μM blebbistatin: transverse scaling exponent (green) and longitudinal scaling exponent (black) (N = 20).

$$\langle \Delta r^2(\tau)\rangle_{\text{passive}} \propto kT\int[1-\exp(-i\omega\tau)]\frac{G''(\omega)}{\omega|G(\omega)|^2}\frac{d\omega}{2\pi} \quad (4)$$

where T is temperature and k is Boltzmann's constant. In Fig. 3B, we plot the sum of active and passive fluctuations (Eqs. 3 and 4) for comparison with our data. We found $\beta = 0.2$ and $\tau_c = 5$ s to result in a good fit of the data after adjusting the amplitudes of both passive and active fluctuations. The motor proteins thus served as multi-timescale probes of cytoskeletal fluctuations. We observed a transition between thermal dynamics in the dominantly elastic cytoskeleton at short times to strongly nonequilibrium power-law dynamics, likely driven by myosin activity, at intermediate times. When the time exceeded the correlation time of the random stress generators, the intermediate regime was followed by a saturation to a maximum MSD, nearly constant over time. Note that in this regime, the MSD amplitude corresponds to a root mean square displacement of ~500 nm (fig. S10), which is larger than the estimated mesh size of the actin network, and thus larger than the expected spacing of obstacles in the crowded cytoplasm.

To investigate whether the transverse nonequilibrium kinesin motor fluctuations were indeed indirectly driven by myosin, we incubated transfected COS-7 cells with blebbistatin and again tracked SWNTs attached to Kif5c kinesin. Blebbistatin is a small-molecule inhibitor of nonmuscle myosin II, blocking myosin in an actin-detached state (*38*, *39*). We used two concentrations, 10 μM and 50 μM blebbistatin, for about 50% and 95% inhibition of myosin (*40*). We again tracked both stationary kinesins and those that moved in a directed manner. MSD analysis showed convergence in the short-time thermal fluctuations as expected, as well as a dose-dependent response in the nonequilibrium section of the MSDs (Fig. 3B). At 10 μM blebbistatin, the amplitude of active stirring was reduced by a factor of ~2, but the exponent $\alpha \approx 1$ was still evident. At 50 μM blebbistatin, the stirring amplitude was suppressed by a further factor of 2, and the MSD exponent decreased, consistent with a substantial suppression of the active stress fluctuations. Tracking of moving motors and separate analysis of on-axis and off-axis MSDs confirmed the suppression of off-axis fluctuations. The exponent decreased to $\alpha \approx 0.6$, whereas on-axis kinesin motility remained largely unaffected (Fig. 4, B and D). There was a slight increase in on-axis motility and a broadening of the velocity distribution (fig. S11), which we speculate might be due to softening of the actin network in the absence of tension (*10*). These results establish nonmuscle myosin II as the dominant driving factor for random cytoskeletal stirring.

Our recordings of kinesin-1 motility in cells over five orders of magnitude in time provide a wide window on intracellular dynamics. We can explain the regimes we observe by a quantitative model of cytoskeletal fluctuations and directed motor motion that describes the transition from thermal motion to nonequilibrium stirring dynamics driven by myosin, as well as the transition from stirring dynamics to directed transport driven by kinesin. Our observations were made possible by the use of SWNT labels for broadband molecular tracking in cells. Many questions concerning motor transport in cells will now be addressable using this approach. We have focused here on the stirring dynamics, which constitute an important mode of active intracellular transport between the limits of random thermal diffusion and directed transport, accelerating nonspecific transport through the nanoporous cytoskeleton.

REFERENCES AND NOTES

1. P. A. Janmey, C. A. McCulloch, *Annu. Rev. Biomed. Eng.* **9**, 1–34 (2007).
2. D. A. Fletcher, R. D. Mullins, *Nature* **463**, 485–492 (2010).
3. F. Huber *et al.*, *Adv. Phys.* **62**, 1–112 (2013).
4. J. Stricker, T. Falzone, M. L. Gardel, *J. Biomech.* **43**, 9–14 (2010).
5. J. Howard, *Mechanics of Motor Proteins and the Cytoskeleton* (Sinauer Associates, Sunderland, MA, 2001).
6. A. Basu, J. F. Joanny, F. Jülicher, J. Prost, *Eur. Phys. J. E* **27**, 149–160 (2008).
7. Y. Tseng, T. P. Kole, D. Wirtz, *Biophys. J.* **83**, 3162–3176 (2002).
8. J. C. Crocker, B. D. Hoffman, *Methods Cell Biol.* **83**, 141–178 (2007).
9. C. P. Brangwynne, G. H. Koenderink, F. C. MacKintosh, D. A. Weitz, *J. Cell Biol.* **183**, 583–587 (2008).
10. D. Mizuno, C. Tardin, C. F. Schmidt, F. C. Mackintosh, *Science* **315**, 370–373 (2007).
11. F. C. MacKintosh, A. J. Levine, *Phys. Rev. Lett.* **100**, 018104 (2008).
12. W. J. Greenleaf, M. T. Woodside, S. M. Block, *Annu. Rev. Biophys. Biomol. Struct.* **36**, 171–190 (2007).

13. C. Leduc, F. Ruhnow, J. Howard, S. Diez, *Proc. Natl. Acad. Sci. U.S.A.* **104**, 10847–10852 (2007).
14. K. J. Verhey, N. Kaul, V. Soppina, *Annu. Rev. Biophys.* **40**, 267–288 (2011).
15. H. Kim, T. Ha, *Rep. Prog. Phys.* **76**, 016601 (2013).
16. B. Huang, H. Babcock, X. Zhuang, *Cell* **143**, 1047–1058 (2010).
17. N. Fakhri, D. A. Tsyboulski, L. Cognet, R. B. Weisman, M. Pasquali, *Proc. Natl. Acad. Sci. U.S.A.* **106**, 14219–14223 (2009).
18. S. M. Bachilo *et al.*, *Science* **298**, 2361–2366 (2002).
19. D. A. Tsyboulski, S. M. Bachilo, R. B. Weisman, *Nano Lett.* **5**, 975–979 (2005).
20. R. B. Weisman, *Anal. Bioanal. Chem.* **396**, 1015–1023 (2010).
21. N. Fakhri, F. C. MacKintosh, B. Lounis, L. Cognet, M. Pasquali, *Science* **330**, 1804–1807 (2010).
22. S. Berciaud, L. Cognet, B. Lounis, *Phys. Rev. Lett.* **101**, 077402 (2008).
23. N. Hirokawa, Y. Noda, Y. Tanaka, S. Niwa, *Nat. Rev. Mol. Cell Biol.* **10**, 682–696 (2009).
24. G. V. Los *et al.*, *ACS Chem. Biol.* **3**, 373–382 (2008).
25. C. P. Brangwynne, G. H. Koenderink, F. C. Mackintosh, D. A. Weitz, *Phys. Rev. Lett.* **100**, 118104 (2008).
26. I. M. Kulic *et al.*, *Proc. Natl. Acad. Sci. U.S.A.* **105**, 10011–10016 (2008).
27. K. Jaqaman *et al.*, *Nat. Methods* **5**, 695–702 (2008).
28. D. Cai, D. P. McEwen, J. R. Martens, E. Meyhofer, K. J. Verhey, *PLOS Biol.* **7**, e1000216 (2009).
29. S. Courty, C. Luccardini, Y. Bellaiche, G. Cappello, M. Dahan, *Nano Lett.* **6**, 1491–1495 (2006).
30. S. Dunn *et al.*, *J. Cell Sci.* **121**, 1085–1095 (2008).
31. Š. Bálint, I. Verdeny Vilanova, Á. Sandoval Álvarez, M. Lakadamyali, *Proc. Natl. Acad. Sci. U.S.A.* **110**, 3375–3380 (2013).
32. C. P. Brangwynne *et al.*, *J. Cell Biol.* **173**, 733–741 (2006).
33. M. Rubinstein, R. Colby, *Polymer Physics (Chemistry)* (Oxford Univ. Press, New York, 2003).
34. B. Fabry *et al.*, *Phys. Rev. Lett.* **87**, 148102 (2001).
35. A. W. C. Lau, B. D. Hoffman, A. Davies, J. C. Crocker, T. C. Lubensky, *Phys. Rev. Lett.* **91**, 198101 (2003).
36. A. J. Levine, F. C. MacKintosh, *J. Phys. Chem. B* **113**, 3820–3830 (2009).
37. This behavior can be understood as follows: The low-frequency behavior, corresponding to times longer than τ_c, is white noise that is independent of frequency, characteristic of uncorrelated fluctuations. For times shorter than τ_c, by contrast, the binding of myosins, subsequent force generation, and eventual release combine to result in a random walk of the net force due to multiple motors in time, with $\langle \Delta f^2(\tau) \rangle \propto \tau$, the Fourier transform of which is $\langle f^2 \rangle_\omega \propto 1/\omega^2$.
38. B. Ramamurthy, C. M. Yengo, A. F. Straight, T. J. Mitchison, H. L. Sweeney, *Biochemistry* **43**, 14832–14839 (2004).
39. A. F. Straight *et al.*, *Science* **299**, 1743–1747 (2003).
40. M. Kovács, J. Tóth, C. Hetényi, A. Málnási-Csizmadia, J. R. Sellers, *J. Biol. Chem.* **279**, 35557–35563 (2004).

ACKNOWLEDGMENTS

We thank L. Cognet, J. Enderlein, M. Guo, J. Lippincott-Schwartz, and D. A. Weitz for helpful discussions; I. Schaap and M. Platen for atomic force microscopy measurements; and the Kavli Institute for Theoretical Physics (University of California, Santa Barbara) for hospitality and useful discussions. Supported by the Center for Nanoscale Microscopy and Molecular Physiology of the Brain and the Collaborative Research Center SFB 937 (Project A2), both funded by the Deutsche Forschungsgemeinschaft, as well as by the Foundation for Fundamental Research on Matter of the Netherlands Organization for Scientific Research, Welch Foundation grant C-1668, and NSF grant NSF PHY11-25915. N.F. was supported by a Human Frontier Science Program Fellowship. N.F. and C.F.S. are inventors on a provisional U.S. patent application on the method used in the paper, filed by Georg-August-Universität. The single-walled carbon nanotubes are available from M.P. under a material transfer agreement with Rice University.

SUPPLEMENTARY MATERIALS

www.sciencemag.org/content/344/6187/1031/suppl/DC1
Materials and Methods
Figs. S1 to S14
Movies S1 to S4
References (*41*–*45*)

24 December 2013; accepted 2 May 2014
10.1126/science.1250170

STRUCTURAL BIOLOGY

Structures of PI4KIIIβ complexes show simultaneous recruitment of Rab11 and its effectors

John E. Burke,[1]*† Alison J. Inglis,[1] Olga Perisic,[1] Glenn R. Masson,[1] Stephen H. McLaughlin,[1] Florentine Rutaganira,[2] Kevan M. Shokat,[2] Roger L. Williams[1]*

Phosphatidylinositol 4-kinases (PI4Ks) and small guanosine triphosphatases (GTPases) are essential for processes that require expansion and remodeling of phosphatidylinositol 4-phosphate (PI4P)–containing membranes, including cytokinesis, intracellular development of malarial pathogens, and replication of a wide range of RNA viruses. However, the structural basis for coordination of PI4K, GTPases, and their effectors is unknown. Here, we describe structures of PI4Kβ (PI4KIIIβ) bound to the small GTPase Rab11a without and with the Rab11 effector protein FIP3. The Rab11-PI4KIIIβ interface is distinct compared with known structures of Rab complexes and does not involve switch regions used by GTPase effectors. Our data provide a mechanism for how PI4KIIIβ coordinates Rab11 and its effectors on PI4P-enriched membranes and also provide strategies for the design of specific inhibitors that could potentially target plasmodial PI4KIIIβ to combat malaria.

Intracellular compartments are essential to eukaryotic cell biology, and both small guanosine triphosphatases (GTPases) and lipids such as phosphoinositides are key components of compartment identity (*1*, *2*). The phosphatidylinositol 4-kinases (PI4Ks) and the small G-protein Rab11 play prominent roles in compartment identity. PI4KIIIβ is one of four mammalian PI4K enzymes that phosphorylate phosphatidylinositol to generate phosphatidylinositol 4-phosphate (PI4P). PI4KIIIβ localizes primarily at the Golgi and is essential for Golgi formation and function (*3*–*5*). PI4P is recognized by protein modules, including the PH domains of oxysterol-binding protein, ceramide transfer protein, and four-phosphate-adaptor protein, that are important for intra-Golgi transport (*6*–*8*). However, typically, lipid recognition alone is not sufficient for Golgi localization, which requires both PI4P and specific small GTPases. In addition to its catalytic role in synthesizing PI4P, PI4KIIIβ also has noncatalytic roles that rely on the interactions with other proteins such as the small GTPase Rab11 (*9*). Rab11 is predominately located on recycling endosomes (*10*). However, Rab11 is also found associated with Golgi membranes, which requires an interaction with PI4KIIIβ (*9*).

PI4KIIIβ activity is essential for replication of a range of RNA viruses, including enteroviruses, SARS coronavirus, and hepatitis C virus (*11*, *12*). These RNA viruses hijack the activity of host cell PI4KIIIβ to generate replication organelles enriched in PI4P. There is no approved antiviral therapy for enteroviruses. However, several compounds inhibit enteroviral replication by targeting cellular PI4KIIIβ (*13*, *14*). PI4KIIIβ is also important in malaria, and inhibitors of *Plasmodium falciparum* PI4KIIIβ are potent antimalarial agents. However, mutations in both PI4KIIIβ and Rab11 confer resistance to these compounds (*15*). Inhibition of *P. falciparum* PI4KIIIβ prevents the membrane ingression that occurs during completion of the asexual erythrocytic stage of the plasmodial life cycle. The role of *Plasmodium* Rab11 and PI4KIIIβ in membrane remodeling is similar to the role of Rab11 and PI4KIIIβ in cytokinesis in *Drosophila* spermatocytes (*16*). In *Drosophila*, PI4KIIIβ is required for the recruitment of both Rab11 and its downstream effectors.

To understand how PI4KIIIβ can both recruit Rab11 and enable its interactions with Rab11 effectors, we used hydrogen-deuterium exchange mass spectrometry (HDX-MS) to facilitate the x-ray crystal structure of human PI4KIIIβ in complex with Rab11a–GTPγS [GTPγS, guanosine 5′-*O*-(3′-thiotriphosphate)] at 2.9 Å resolution (see supplementary materials and methods). To form crystals, highly flexible regions of PI4KIIIβ identified by HDX-MS were truncated (residues 1 to 120, 408 to 507, and 785 to 801) (Fig. 1A). This included a C-terminal region necessary for catalytic activity (fig. S2A). The PI4KIIIβ structure consists of two domains, a right-handed helical solenoid (residues 128 to 243) and a kinase domain (residues 306 to 801) (Fig. 1B), that are related to the PI3Ks (fig. S3). The kinase domain has two lobes, an N-terminal lobe dominated by a five-stranded antiparallel β sheet and a C-terminal lobe that is largely helical, with the adenosine triphosphate (ATP)–binding site located in a cleft between the lobes. The N lobe of PI4KIIIβ has a PI4KIIIβ-distinct, large insertion (residues 391 to 539) (Fig. 1B).

[1]Medical Research Council (MRC) Laboratory of Molecular Biology, Cambridge CB2 0QH, UK. [2]Howard Hughes Medical Institute and Department of Cellular and Molecular Pharmacology, University of California, San Francisco (UCSF), San Francisco, CA 94158, USA.
***Corresponding author. E-mail: jeburke@uvic.ca (J.E.B.); rlw@mrc-lmb.cam.ac.uk (R.L.W.)** †Present address: Department of Biochemistry and Microbiology, University of Victoria, Victoria, British Columbia, Canada.

Science

High-resolution mapping of intracellular fluctuations using carbon nanotubes

Nikta Fakhri, Alok D. Wessel, Charlotte Willms, Matteo Pasquali, Dieter R. Klopfenstein, Frederick C. MacKintosh and Christoph F. Schmidt

Science **344** (6187), 1031-1035.
DOI: 10.1126/science.1250170

Motors stirring within the living cell

Cytoskeletal dynamics is key to cellular function. At very short time scales, thermal motions probably dominate, whereas on time scales from minutes to hours, motor-protein-12–based directed transport is dominant. But what about the times in between? Fakhri *et al.* tracked kinesin molecules labeled with carbon nanotubes and monitored their motion in living cells for milliseconds to hours. The kinesins motored along microtubule tracks, but sometimes moved more randomly as the tracks themselves were moved by active, larger-scale cell movements. This active "stirring" of the cytoplasm may play a role in nonspecific transport.

Science, this issue p. 1031

Science (print ISSN 0036-8075; online ISSN 1095-9203) is published by the American Association for the Advancement of Science, 1200 New York Avenue NW, Washington, DC 20005. The title *Science* is a registered trademark of AAAS.